Acta Geochim (2017) 36(1):74–88
DOI 10.1007/s11631-016-0126-2

ORIGINAL ARTICLE

The Harrat Al-Birk basalts in southwest Saudi Arabia: characteristic alkali mafic magmatism related to Red Sea rifting

Rami A. Bakhsh[1]

Received: 17 June 2016 / Revised: 31 July 2016 / Accepted: 19 September 2016 / Published online: 24 September 2016

Abstract Harrat Al-Birk volcanics are products of the Red Sea rift in southwest Saudi Arabia that started in the Tertiary and reached its climax at ~5 Ma. This volcanic field is almost monotonous and is dominated by basalts that include mafic–ultramafic mantle xenoliths (gabbro, websterite, and garnet-clinopyroxenite). The present work presents the first detailed petrographic and geochemical notes about the basalts. They comprise vesicular basalt, porphyritic basalt, and flow-textured basalt, in addition to red and black scoria. Geochemically, the volcanic rock varieties of the Harrat Al-Birk are low- to medium-Ti, sodic-alkaline olivine basalts with an enriched oceanic island signature but extruded in a within-plate environment. There is evidence of formation by partial melting with a sort of crystal fractionation dominated by clinopyroxene and Fe–Ti oxides. The latter have abundant titanomagnetite and lesser ilmenite. There is a remarkable enrichment of light rare earth elements and depletion in Ba, Th and K, Ta, and Ti. The geochemical data in this work suggest Harrat Al-Birk basalts represent products of water-saturated melt that was silica undersaturated. This melt was brought to the surface through partial melting of asthenospheric upper mantle that produced enriched oceanic island basalts. Such partial melting is the result of subducted continental mantle lithosphere with considerable mantle metasomatism of subducted oceanic lithosphere that might contain hydrous phases in its peridotites. The fractional crystallization process was controlled by significant separation of clinopyroxene followed by amphiboles and Fe–Ti oxides, particularly ilmenite. Accordingly, the Harrat Al-Birk alkali basalts underwent crystal fractionation that is completely absent in the exotic mantle xenoliths (e.g. Nemeth et al. in The Pleistocene Jabal Akwa Al Yamaniah maar/tuff ring-scoria cone complex as an analogy for future phreatomagmatic to magmatic explosive eruption scenarios in the Jizan Region, SW Saudi Arabia 2014).

Keywords Harrat Al-Birk · Alkaline basalt · Red Sea rifting · Hydrous mantle · Reworked oceanic crust

1 Introduction

The Phanerozoic volcanic rocks of the Saudi Harrats were generated by the Oligo-Miocene initiation of the Red Sea that produced large amounts of lithospheric melts, including various lava flows of olivine basalt and hawaiite, in addition to mugearite, trachyte, and benmorite (Healy et al. 1982; Coleman et al. 1983; Brown et al. 1989).

Various studies have been conducted on different aspects of the volcanic rocks of the Saudi Harrats, including their origin. According to Moufti et al. (2011 and 2012), the magmas of the Saudi Harrats were possibly generated by partial melting provoked by lithospheric thinning caused by Red Sea rift tectonics. Recently, Surour and Moufti (2013) used opaque minerals, particularly spinel, to trace the magmatic history of the Saudi Harrats volcanics, assessing volcanic hazards (Moufti and Hashad 2005) and establishing a geoparks grouping system to increase awareness of the hazards (Moufti et al. 2013). Studies have also been conducted on the rocks' petrogenesis (e.g. Coleman et al. 1977). The mantle xenoliths for

✉ Rami A. Bakhsh
rami_bk@yahoo.com

[1] Department of Mineral Resources and Rocks, Faculty of Earth Sciences, King Abdulaziz University, P.O. Box 80206, Jeddah 21589, Saudi Arabia

the latest rocks are mainly spinel peridotite and spinel pyroxenite, while the mantle xenoliths of the first type are mainly composed of websterites, garnet clinopyroxenites, and pyroxene gabbros. Mantle xenoliths indicate a different tectonic environment for the origin of the western Arabian lower crust (generated from a convergent plate margin) compared to the eastern (originated from a hotspot) (Nasir and Stern 2012).

The post-Miocene Phanerozoic volcanic rocks at Harrat Al-Birk (Fig. 1) are on the southwestern part of the Arabian Shield, between Wadi Hali and Wadi Nahb, parallel to the Red Sea coastal plain. They are characterized by circular feeder pipes and deeply dissected small cinder cones, and are dominantly north-trending (Coleman et al. 1983), extending along the Red Sea shore north of the Ad Darb fault and north Jizan. The rocks overlay Precambrian crust (Nemeth et al. 2014), and display irregular elongate flows that cover nearly 1800 km^2, and are up to 150 m high and 800 m in diameter (Coleman et al. 1983).

The present paper focuses on the classification of the poorly studied basaltic flows of the Harrat Al-Birk in terms of mineralogy and geochemistry. These basaltic flows contain fine-grained spinel, a significant indicator of the magma source. Our detailed geochemical and petrological analyses were conducted with the goals of (1) identifying petrographic varieties in different Harrat Al-Birk basaltic flows, (2) determining the main mineralogical and geochemical characteristics of the basaltic rocks, and (3) precisely determining the magma source. Our findings illuminate the processes and conditions of formation of the area of interest, and contribute to an improved understanding of the lithospheric evolution beneath the Arabian shield.

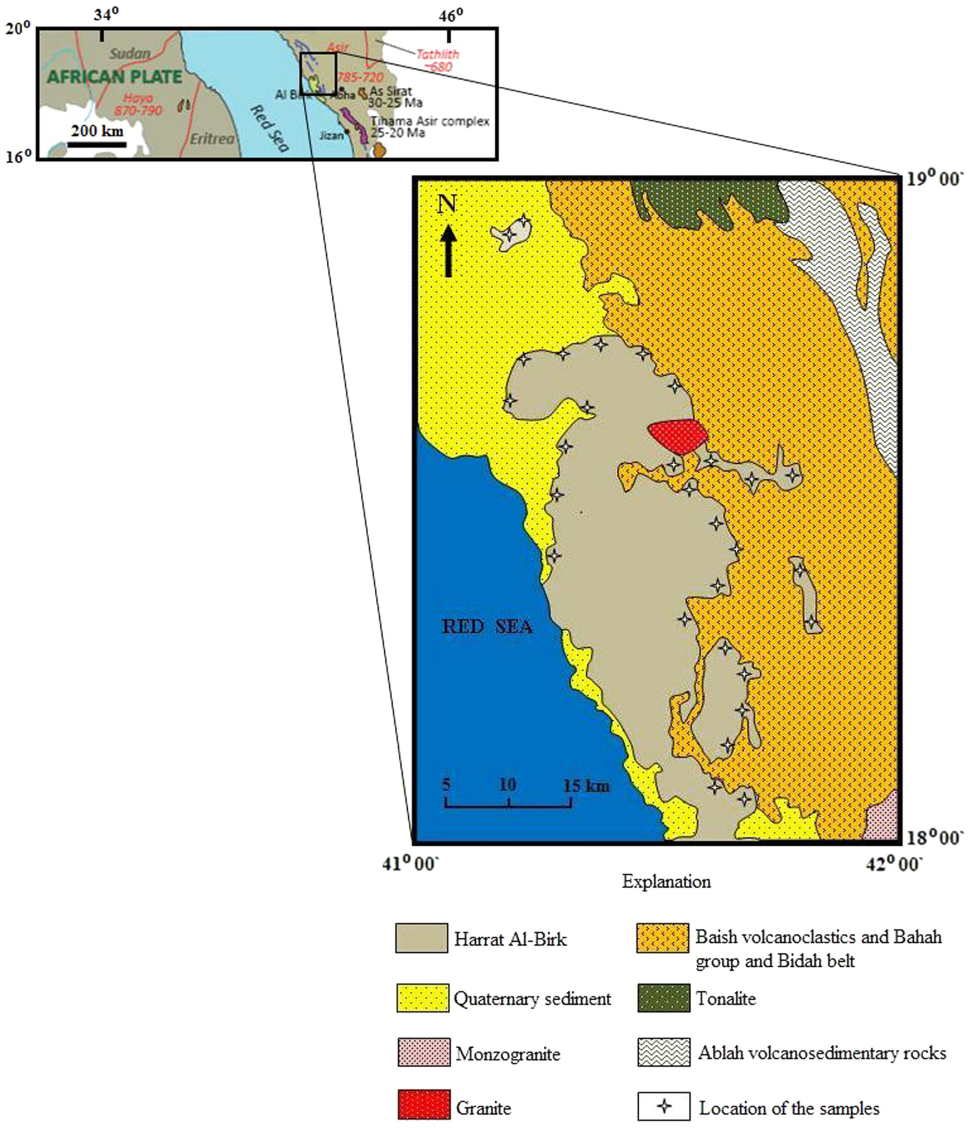

Fig. 1 Harrat Al-Birk geological map (modified after Nemeth et al. 2014)

Fig. 2 Rock types, structures, and rock relationships

2 Methodology

Our work included an extensive literature review, field observations, and sample location identification using topographic sheets and modern satellite images. Fieldwork included sampling basaltic flows and other rock varieties. Transmitted- and reflected-light microscopy was used for identification of minerals, textures, and microfabrics. Whole-rock geochemistry was analyzed in the context of its significance for the petrogenesis of the studied volcanic and the implication on mafic magmatism during rift of the southern Red Sea. Geochemical analyses were performed at the ACME Analytical Laboratories Ltd., Canada. Major elements, Sc, Ba, and Ni concentrations were determined by inductively coupled plasma-atomic emission spectrometry (ICP-AES) after fusing 0.2 g of sample powder using $LiBO_2$. Other trace elements including rare earth elements (REEs) were determined by inductively coupled plasma-mass spectrometry (ICP-MS).

3 Geologic set up and field observations

The Harrat Al-Birk post-Miocene volcanics are represented by circular feeder pipes and deeply dissected small cinder cones (Coleman et al. 1983). They extend along the Red Sea coast on Precambrian crust (Nemeth et al. 2014). The

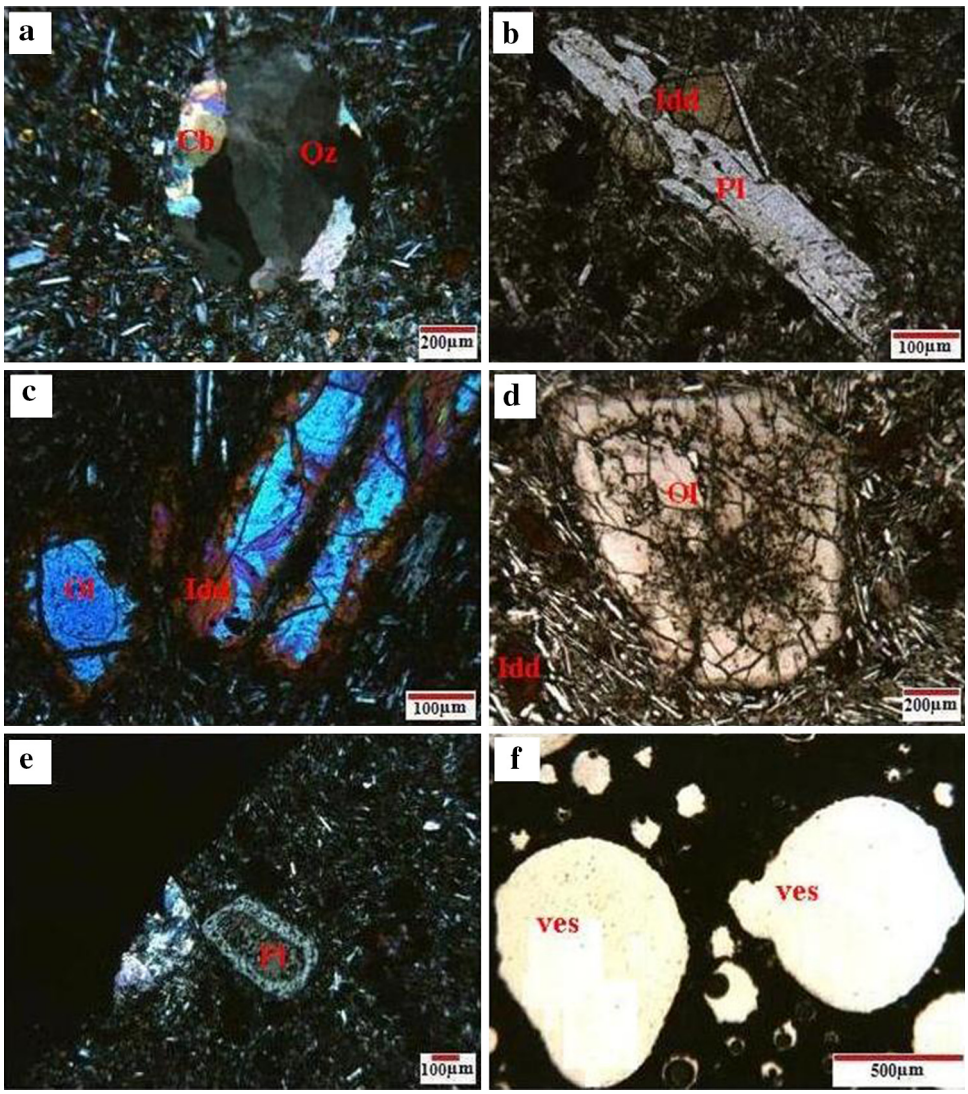

Fig. 3 Photomicrographs showing mineral assemblages and textures **a** vesicles filled by quartz and carbonate, amygdaloidal texture (CN), **b** olivine crystal partially corroding and/or replacing plagioclase (PPL), **c** olivine phenocrysts altered to iddingsite along peripheries and cracks (CN), **d** porphyritic texture showing *Y-shaped* cracks in olivine phenocrysts that enclose fine crystals of quartz and iron oxides in PPL, **e** zoned plagioclase phenocryst surrounded by altered olivine in XPL, **f** empty vesicles, vesicular texture (PPL)

Precambrian basement at the eastern side of the north part of the area is invaded by Tertiary diabase dikes that underlie the Harrat Al-Birk flows to the south with a distinct unconformable relationship. The Harrat Al-Birk volcanics cap the Jabal at Tirf dike swarm and Wajid Sandstone to the west where the volcanics flowed over exhumed coral reefs (Coleman et al. 1983). Some recent studies (e.g. Nemeth et al. 2014) attribute the Harrat Al-Birk volcanics to the Tertiary-to-recent continental axial rifting in the Red Sea axial trough, which is believed to have an active status. This type of recent rift-related mafic magmatism (~5 Ma) also includes subalkaline oceanic tholeiites (Ross et al. 1973). There is a dissimilarity to volcanism in the majority of the Arabian Shield, Ethiopia, and Yemen. Such Tertiary volcanics are characterized by accumulations of undersaturated alkali basalts (Baker et al. 1973).

According to Coleman et al. (1983), the Harrat Al-Birk flows are mostly blocky on their upper surfaces and interbedded with pyroclastics, columnar in the lower part but knobby in the upper part. The Harrat Al-Birk ultramafic and mafic xenoliths provide significant clues of the formational processes of the Red Sea margin (McGuire 1988). The xenoliths are mainly composed of websterites (spinel-plagioclase-amphibole-olivine assemblages), garnet clinopyroxenite, and two-pyroxene gabbro (olivine). The mafic and ultramafic inclusions of Harrat Al-Birk represent two episodes of volcanism: the Miocene eruption which is characterized by only harzburgite inclusions; and the Precambrian eruption which, in contrast, has a variety of inclusions, namely harzburgites, cumulate gabbro, and websterite, associated with glassy alumina-rich clinopyroxene, plagioclase, and spinel phenocrysts, which originated from thicker crust than the younger eruption (Nemeth et al. 2014). Exotic

xenoliths in the Harrat Al-Birk mafic volcanics have been reported in various studies (Ghent et al. 1979; Healy et al. 1982). Nemeth et al. (2014) subdivided the Precambrian inclusions of the Harrat Al-Birk into two phases of emplacement: the Clinopyroxene and plagioclase megacrysts young phase that formed at shallower depth (<35 km), and the old phase of layered websterites and gabbros associated with cumulate plagioclase and clinopyroxene that formed deep in the lower crust. McGuire (1988) found the garnet clinopyroxenite is characterized by Fe–Al-rich rims on the clinopyroxene and reaction rims on the garnet which they attributed to formation under elevated temperature.

Urban development has limited the number of accessible locations in the Harrat Al-Birk volcanics. However, field observations support the established finding that the volcanic activity of the Harrat Al-Birk includes both volcanic flows and pyroclastics.

The basaltic flows include various textures (Fig. 2): vesicular, blocky, sheet-like, knobby-like, columnar, and bedded, while the pyroclastics are dominated by almond-form bombs, welded fragments and agglomerate, stretched pebbles, and irregular lightweight reddish scoria. The field relationships (Fig. 2) indicate that the basaltic blocky form is found at the highest part of the flows that are sometimes interbedded with pyroclastic products, and overlies sedimentary rocks. Columnar joints are exposed in a few valleys, with an upper zone of knobby rock. Nearby, fractured volcanics with clear graded bedding were traced, but showed no clear relationship with other rock types. The pyroclastics were sometimes observed in carbonates associated with coral reefs.

Although a large number of scoria cones were observed, few were accessible because they are mostly in the inner part of the Harrat Al-Birk, surrounded by fence panels.

4 Petrography

This section is devoted to the petrographic characterization of the studied basaltic rocks from the Harrat Al-Birk (Fig. 3). Differences in mineralogy and textural varieties are presented. Petrographic descriptions of each variety follow.

4.1 Vesicular basalt

Voids in sampled vesicular basalt amount to up to ~25 % of total volume, and the vesicles attain a diameter as wide as 2500 μm. The rock consists of olivine, plagioclase, clinopyroxene, and Fe–Ti oxides. Sometimes vesicles are filled by calcite, forming a diagnostic amygdaloidal texture. This basaltic variety is characterized by remarkably coarse olivine phenocrysts up to ~300 μm long. These olivine crystals have a common skeletal nature and are arrow-headed. Along outer peripheries, olivine is altered to iddingsite, forming rim placement texture at places where pervasive alteration has proceeded inwards. Finer olivine crystals are occasionally gathered to form a micro-glomeroporphyritic texture. Brown spinel inclusions are commonly encountered in the olivine crystals, especially at the cores of coarse phenocrysts. Plagioclase occurs as microlites that are interstitial to olivine and vesicles. The extremely fine plagioclase lathes are up to 160 μm long and as little as ~10 μm wide and display flow texture in some instances.

4.2 Black and red scoria

The scoriaceous basalts in the area of study are characterized by abundant vesicles (~65 %). The vesicles are almost equant and rounded but occasional lenticular ones were also recorded. Occasional amygdules are present with the vesicles filled by calcite and to lesser extent by silica. The size of vesicles varies greatly with a range of 50–1300 μm. Plagioclase in the samples is microlitic and its length averages ~200 μm with some up to 1200 μm long. The plagioclase/olivine ratio is about 1.5. Olivine crystals are fine and they are mostly subhedral with frequent bi-pyramidal terminations and partial replacement to iddingsite along cracks and peripheries. Magnetite (the only Fe–Ti oxide observed) is extremely fine and amounts to ~10 %–12 % of total rock volume. In some weathered samples, the magnetite is replaced by Fe-oxyhydroxide in the form of possible goethite and limonite.

4.3 Porphyritic basalt

The most characteristic feature in sampled porphyritic basalt is the abundant occurrence of olivine and plagioclase phenocrysts that give the rock a very distinct porphyritic nature. Recognition of that porphyritic nature is not observed microscopically only but by the naked eye as well. Olivine phenocrysts (up to 850 μm along and ~400 μm wide) are mostly fresh, but are partially replaced by iddingsite in a way similar to the previously described basaltic varieties. In some instances, coarse olivine phenocrysts engulf plagioclase due to peripheral embayment. Some samples contain shattered olivine crystals that might represent xenocrystic mantle phases. These never possess straight or subhedral outlines as the other olivine phenocrysts do. Sometimes, the plagioclase phenocrysts are zoned and equant (~470 μm wide). In addition to coarse plagioclase phenocrysts, microlitic plagioclase is also seen. Optically, both plagioclase phenocrysts and microlites are anorthitic to andesine, though

Table 1 Chemical analyses of the major oxides (in wt%) and the trace and rare earth elements (in ppm) of the Harrat Al-Birk volcanic rocks

Sample	BPor-B1	BPor-B2	BPor-B3	BPor-B4	BPor-B5	BPor-B6	BF-t B1	BF-t B2	BF-t B3	BF-t B4	BF-t B5
Major oxides											
SiO_2	43.66	45.07	43.84	45.17	44.68	44.67	43.89	47.08	47.39	43.73	44.42
TiO_2	2.84	2.02	2.88	2.03	2.08	2.19	3.49	2.22	2.22	3.49	2.83
Al_2O_3	14.48	14.62	15.58	14.68	14.69	14.43	16.45	16.36	16.54	16.31	15.88
Fe_2O_3	12.62	11.72	13.09	13.04	11.48	12.7	13.75	9.9	9.76	14.05	12.53
MnO	0.18	0.18	0.19	0.22	0.18	0.2	0.21	0.17	0.16	0.21	0.19
MgO	10.24	8.7	6.86	7.82	8.05	9.15	5.8	7.72	6.48	5.41	6.99
CaO	10.17	10.8	10.56	9.09	11.77	9.43	9.3	8.95	9.22	9.24	10.16
Na_2O	3.03	3.03	2.36	3.37	2.98	3.14	3.34	3.76	3.87	3.56	3.04
K_2O	0.45	0.77	0.82	1.08	0.86	1.01	1.14	1.37	1.62	1.14	1
P_2O_5	0.46	0.38	0.5	0.78	0.42	0.64	0.77	0.61	0.61	0.81	0.66
LOI	1.34	1.69	2.65	2.12	2.45	1.96	1.01	1.17	1.74	1.25	1.46
Total	99.58	99.13	99.45	99.51	99.75	99.64	99.22	99.42	99.69	99.3	99.26
Trace elements											
Ba	332	800	751	530	352	411	632	608	414	416	453
Hf	3.9	3.9	5	4.9	4.6	4.8	5.5	5.3	5.4	5.2	4.8
Nb	35.1	30.1	39.7	40.8	33.5	39.7	48.1	53.3	52	48.4	41
Rb	6.6	15	15.8	20.9	17.2	18.8	17.1	28.4	32.8	17.9	17.3
Sr	632.7	697.1	784.9	817.1	549.5	757.3	980	824.9	760	910.7	750.9
Ta	2.2	1.9	2.4	2.5	2.3	2.2	2.8	3.3	3.1	3	2.1
Th	2.4	3	3	2.8	3.1	3.1	3.1	5.1	4.5	3	3.1
U	0.6	0.7	1.1	0.9	0.9	0.8	0.8	1.9	1.3	0.9	0.8
V	299	267	301	170	248	197	267	226	211	234	242
Zr	173.8	161.7	213.6	231.8	181.8	204.7	229	257.4	248.1	224.1	186.9
Y	25.4	24.9	29.4	25.7	24.3	26.5	33.1	27.1	26.4	30.7	26.7
Ni	208	198.4	159.6	158.4	195.5	187.9	37.3	111.4	95.5	33.1	112.3
Cu	71.5	73.3	68.9	64.6	63.5	58.4	45.5	50.2	46.4	52.4	58.4
As	0.5	1	0.7	0.6	0.8	0.6	1	1.6	1.2	0.7	1
Rare earths											
La	26.2	24.1	33.7	36.3	28.7	33.4	35.6	40.2	38.9	34.6	33.6
Ce	59.8	52	65.8	74.9	57.2	68.5	79.1	82.6	78.8	78.1	67.5
Pr	7.1	6.18	8	8.59	6.67	8.23	9.66	9.01	8.69	9.32	8.26
Nd	29.7	24.9	35.4	33.9	26	33.6	40.7	32.6	33.9	39.4	34.5
Sm	5.88	5.23	7.33	6.69	5.32	6.61	8.52	6.86	6.57	8.16	7.22
Eu	1.98	1.83	2.31	2.31	1.87	2.2	2.91	2.26	2.08	2.73	2.28
Gd	6.08	5.37	6.87	6.47	5.21	6.35	8.07	6.19	6.22	7.88	6.75
Tb	0.9	0.8	1.02	0.92	0.83	0.95	1.2	0.89	0.91	1.23	0.98
Dy	5.08	4.59	5.77	5.13	4.53	5.36	6.28	5.52	5.16	6.29	5.46
Ho	0.96	0.86	1.14	0.95	0.95	0.99	1.24	0.97	0.96	1.19	1.07
Er	2.62	2.4	2.88	2.63	2.46	2.94	3.33	2.8	2.8	3.31	2.65
Tm	0.33	0.35	0.39	0.37	0.35	0.41	0.46	0.39	0.4	0.44	0.38
Yb	2.13	2.21	2.36	2.3	2.28	2.49	2.71	2.31	2.74	2.77	2.4
Lu	0.32	0.35	0.36	0.37	0.33	0.36	0.42	0.4	0.38	0.39	0.38

Sample	BVB1	BVB2	BVB3	BRS	BAB
Major oxides					
SiO_2	44.18	44.57	44.33	43.31	45.56
TiO_2	2.15	2.55	3.43	2.77	3.35
Al_2O_3	14.89	15.58	16.63	16.07	16.78

Table 1 continued

Sample	BVB1	BVB2	BVB3	BRS	BAB
Fe_2O_3	12.64	12.05	14.27	13.51	13.87
MnO	0.21	0.23	0.22	0.2	0.21
MgO	6.39	6.75	4.8	7.26	4.05
CaO	9.72	9.94	8.3	7.77	7.89
Na_2O	3.29	2.76	3.71	2.14	4.25
K_2O	1.09	0.87	1.31	0.88	1.49
P_2O_5	0.65	0.63	0.67	0.64	0.57
LOI	4.1	2.94	1.27	4.91	1.07
Total	99.44	99.23	99	99.55	99.19
Trace elements					
Ba	458	2945	658	340	711
Hf	5	5	5.8	5.4	6.4
Nb	38.8	44.6	51.5	48.8	57.3
Rb	18.1	13.2	21.5	6.1	25.3
Sr	658.6	812	907.8	571.7	936
Ta	2.3	2.9	3.2	3.2	3.3
Th	3.1	3.7	3.6	3.9	3.8
U	0.5	0.7	1.1	0.5	1.2
V	155	231	223	233	200
Zr	207.5	222.5	250	243.9	272.7
Y	27.2	27.1	34.7	30.3	34.4
Ni	152.1	133.3	29.9	131.9	10.1
Cu	90.5	66.6	41.8	88.8	36.9
As	<0.5	1	1.4	0.9	1.1
Rare earths					
La	34.3	37.6	39	38.3	41.5
Ce	71	76.4	79.7	78.6	87.5
Pr	8.53	8.76	10.23	9.1	10.7
Nd	32.3	34.8	41.3	38.3	44.8
Sm	6.87	7.04	8.63	7.6	8.79
Eu	2.14	2.34	2.91	2.45	2.95
Gd	6.28	6.62	8.03	7.07	8.61
Tb	0.94	1.02	1.2	1.08	1.2
Dy	5.69	5.33	6.67	5.31	6.87
Ho	0.91	1.03	1.28	1.11	1.37
Er	2.53	2.65	3.49	2.95	3.72
Tm	0.38	0.37	0.48	0.43	0.48
Yb	2.35	2.42	2.92	2.47	3.37
Lu	0.36	0.35	0.44	0.4	0.51

Major elements, Ba, and Ni concentrations determined by inductively coupled plasma-atomic emission spectrometry (ICP-AES) after fusing 0.2 g of sample powder using $LiBO_2$

Other trace elements including REE were determined by inductively coupled plasma-mass spectrometry (ICP-MS)

Explanation for the symbols: *BPor-B1 to BPor-B6* porphyritic basalt, *BF-t B1 to BF-t B5* flow-textured basalt, *BVB1 to BVB3* Vesicular basalt, *BRS* red scoria

this should be verified by electron microprobe spot analyses. Occasional augite occurs in the porphyritic basalt; some stout crystals attain the size of a phenocryst and display zoning and to a lesser extent lamellar twinning.

4.4 Flow-textured basalt

Flow texture is the basis of this rock variety's nomenclature. It can be easily identified by the perfect alignment

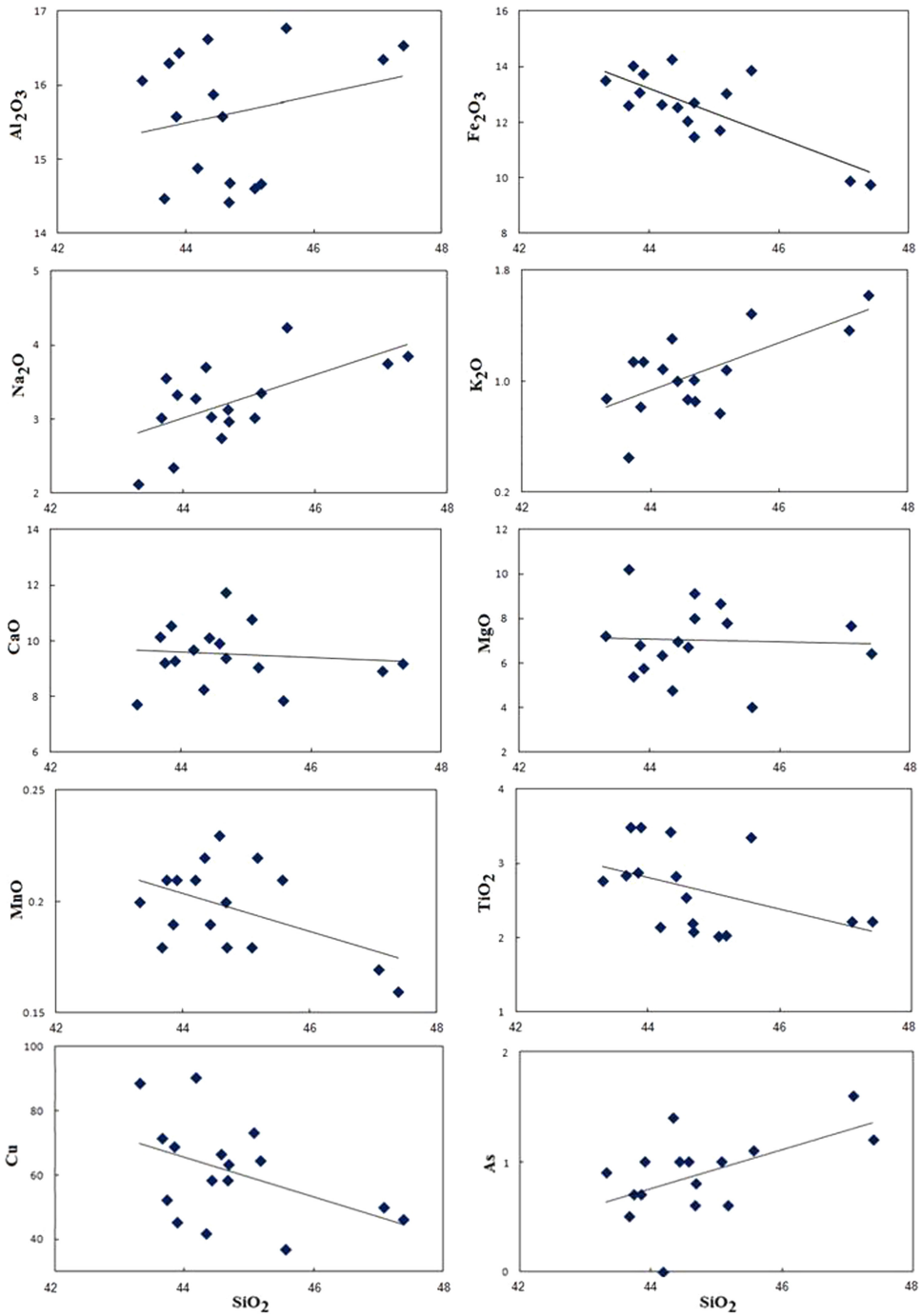

Fig. 4 Major oxides and some trace oxides versus SiO_2 (wt%) for the Harrat Al-Birk volcanics

of plagioclase lathes. On a microscopic scale only, the rock can be considered porphyritic. The size of olivine micro-phenocrysts is noticeably greater than that of plagioclase (up to 950 and 270 μm long, respectively). Amygdules (carbonate-bearing) are very few but distinctly wide (up to ~3200 μm). Interstitial carbonate (calcite) was also recorded. Olivine is mostly skeletal with abundant spinel inclusions. Another finer and younger generation of olivine as a groundmass component is also present, with complete replacement by iddingsite. Augite is the sole clinopyroxene phase that occurs as a groundmass component. It is commonly altered to actinolite and chlorite, but some fresh relics survive. Few zoned plagioclase crystals are present; frequent Fe–Ti oxides (magnetite + ilmenite) display a distinct skeletal habit and high degree of freshness.

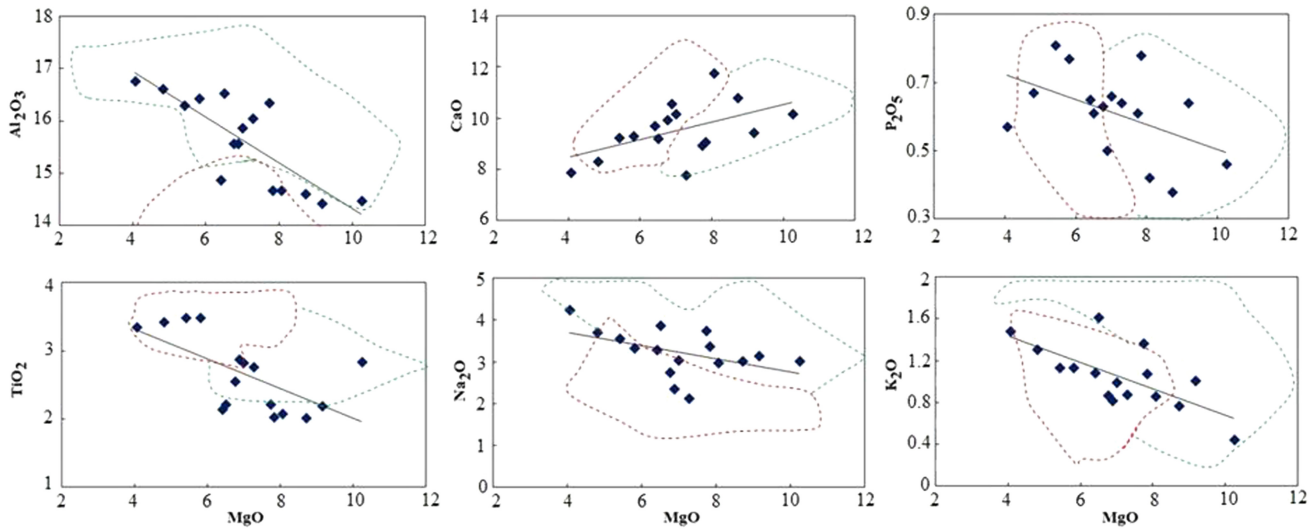

Fig. 5 Major oxides versus MgO (wt%) for the Harrat Al-Birk volcanic rocks. The fields of Ethiopian (*red line-dashed area*) and Saudi Arabian (*green line-dashed area*) basalts are shown for comparison (Mattasah et al. 2013)

5 Geochemistry

The major, trace, and rare earth elements of the Harrat Al-Birk are shown in Table 1. Generally, the concentrations of the major elements in the Harrat Al-Birk volcanics show some variability (Table 1). There is a range of silica content (from 43.31 % to 47.39 %) which indicates more or less a fractional character. The variability in chemistry is clear in analyses of Fe_2O_3 (9.76 %–14.27 %), MgO (4.05 %–10.24 %), and CaO (7.71 %–11.77 %), while less variability was observed in TiO_2 (2.14 %–3.32 %), Na_2O (2.14 %–4.25), K_2O (0.45 %–1.49 %), and P_2O_5 (0.38 %–0.81 %). The LOI values of the Harrat Al-Birk basalts range from 1.01 % to 4.91 %. Such a wide range is thought to be due to carbonate minerals in the vesicular samples. In order to demonstrate general trends of composition with respect to these elements, some diagrams (Figs. 4, 5) were constructed of major oxides and trace elements plotted against SiO_2 and MgO. The plots of major and trace elements versus SiO_2 (Fig. 4) show clear negative correlations of silica against ferric Fe, Ti, and Cu, and show a clear positive correlation against Na, K, and As. The figures show no distinct correlation in the cases of both Ca and Mg. The Harrat Al-Birk basalts are comparable to intra-plate basalts in Ethiopia in terms of the plot of MgO versus some major oxides and also display similarity to the rest of Saudi Harrat volcanic fields (Mattasah et al. 2013) as shown in Fig. 5.

For the purpose of rock classification, the following diagrams were created: the $Na_2O + K_2O$ versus SiO_2 (TAS) diagram of Le Bas et al. (1986) (Fig. 6a), the Zr/TiO*0.0001 versus Nb/Y diagram of Winchester and Floyd (1977) (Fig. 6b). For chemical characterization, the SiO_2 versus TiO_2 diagram after Ulrych et al. (2010) (Fig. 7a), the K_2O versus Na_2O diagram after Middlemost (1975) (Fig. 7b), and the alkali versus silica diagram after Murcia et al. (2013) (Fig. 7c) were constructed. In Fig. 4b, the variation of Ti is a function of the primary melt from which basalt is derived and of the amount of the element incorporated in Fe–Ti oxides and in clinopyroxene (titanaugite). The characterization (Figs. 6, 7) indicates that the studied volcanic rocks are low- to medium-Ti, sodic-AOB. The studied AOBs show a differentiation trend (Fig. 6a, b).

For tectonomagmatic determination, the TiO_2-MnO*10-P_2O_5*10 diagram (after Mullen 1983) (Fig. 8a), the Zr/4-Y-Nb*2 diagram of Meschede (1986) (Fig. 8b), the Z versus Zr/Y diagram of Pearce and Norry (1979) (Fig. 8c), and the TiO_2 versus Y/Nb diagram (after Floyd and Winchester 1975) (Fig. 8d) were used. Figure 8a–d suggests a within-plate environment for the basalts of the Harrat Al-Birk. In Fig. 8d, although the samples of basalt fit well with the continental alkali basalt field, they also plot along the boundaries between oceanic alkali and the continental tholeiitic basalt fields, and within the oceanic alkali basalt field, which accommodate the highest Zr/Y ratios of Pearce and Norry (1979) (Fig. 8c). The Harrat Al-Birk basalts are thus proposed to have formed in an intra-plate setting rather than in mid-ocean ridge basalt (MORB) or Island Arc settings. The same conclusion was reached using the Floyd and Winchester (1975) diagram, which is used to differentiate various tectonic settings: the Harrat Al-Birk basalt samples are confined to the continental alkali basalt field (Fig. 8d).

For comparison, various diagrams, namely $Na_2O + K_2O$ versus SiO_2 (Fig. 9), Nb/Y versus Zr/Y, variability displayed by the studied basalts, and reference

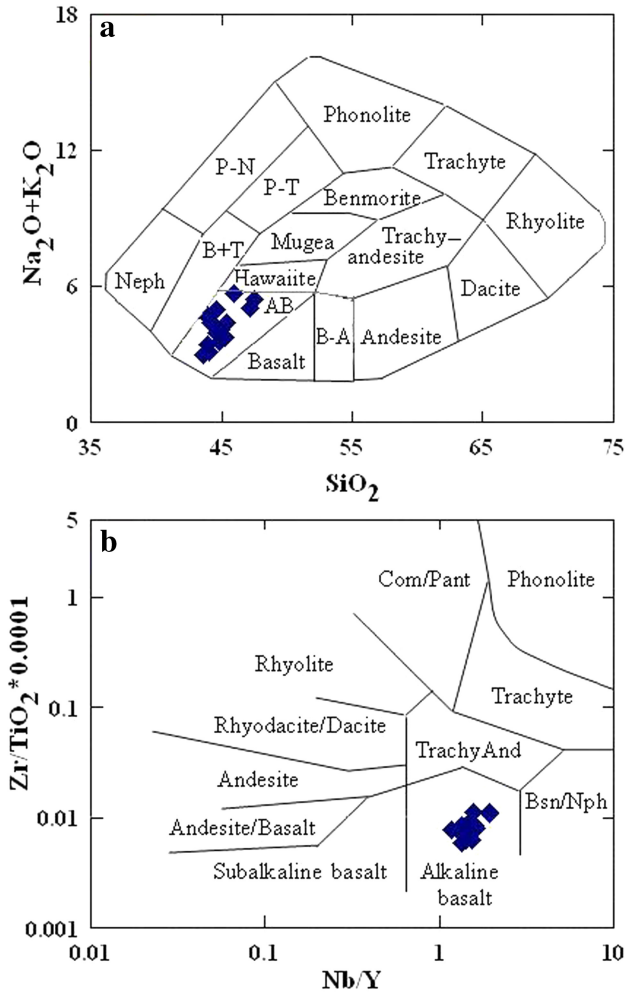

Fig. 6 Rock nomenclature diagrams **a** $Na_2O + K_2O$ versus SiO_2 (TAS) diagram of Le Bas et al. (1986) and **b** $Zr/TiO_2*0.0001$ versus Nb/Y diagram of Winchester and Floyd (1977). Symbol explanation is given in Fig. 1

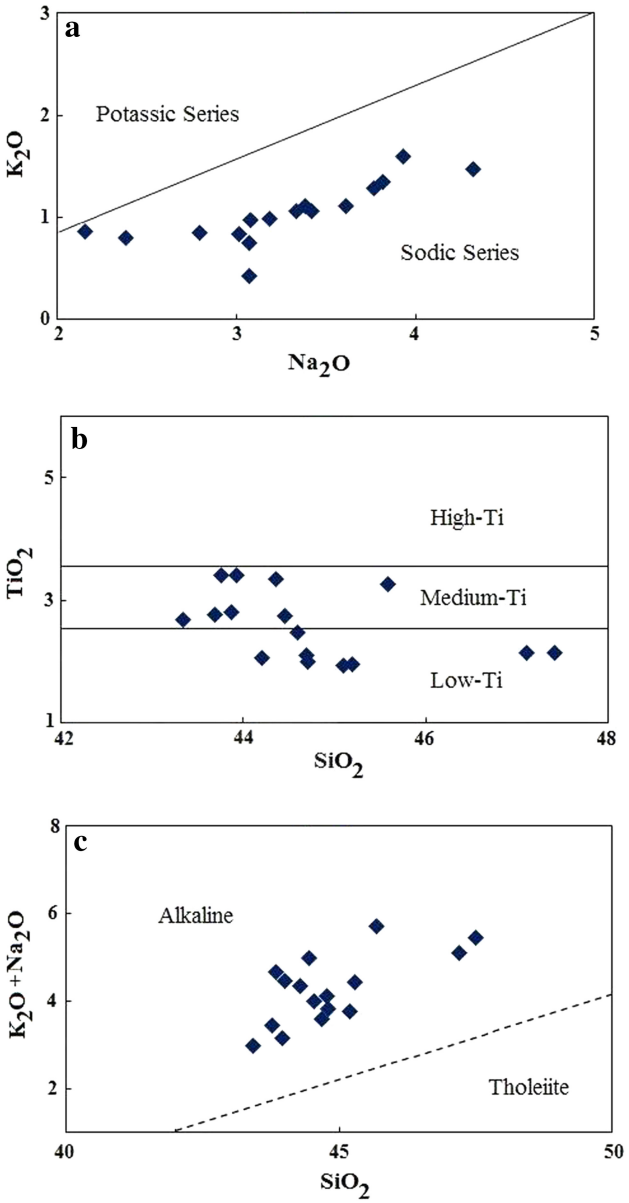

Fig. 7 Rock characterization diagrams **a** SiO_2 versus TiO_2 after Ulrych et al. (2010), **b** K_2O versus Na_2O after Middlemost (1975), **c** Alkali vs. Silica after Murcia et al. (2013). The symbols in the diagrams represent the basalts of the Harrat Al-Birk

analyses from Fitton and James (1986) suggest there is a distinct Iceland array (Fig. 10a). Further, a Ce/U versus Nb/U diagram (Fig. 10b) shows a comparison with an average MORB crust (Hofmann et al. 1986; Ito et al. 1987) and ocean island basalt (OIB) (Hofmann et al. 1986; Davies et al. 1989), and a primitive mantle-normalized traces diagram with normalization after Sun and McDonough (1989) (Fig. 10c). Other comparisons used were (1) chondrite-normalized REE-incompatible REE element values of the studied basalts and those of the average OIB (Sun and McDonough 1989), (2) average N-type MORB (Sun and McDonough 1989), (3) OIB and AOB analyses from Camp and Roobol (1989) (Fig. 10d), (4) Sr versus Zr (Fig. 10e) and Ni versus V (Fig. 10f) for possible partial melting and fractionation paths (from Camp and Roobol 1989), and (5) Th/Yb versus SiO_2 (Fig. 10g) and Th/Yb versus Nb/Yb (Fig. 10h) after Pearce and Peate (1995) to identify any possible crustal contamination and fractionation effects.

Petrogenetically, the characterization of the source and the possible processes of formation were identified by implementing a comparison between certain element ratios and well-known sources (Fig. 10a, b). The chondrite-normalized rare earth diagram (Fig. 10d) clearly shows light REE/heavy REE enrichment with a consistent slope, absent the Eu anomaly and slight anomalies for Dy and Sm.

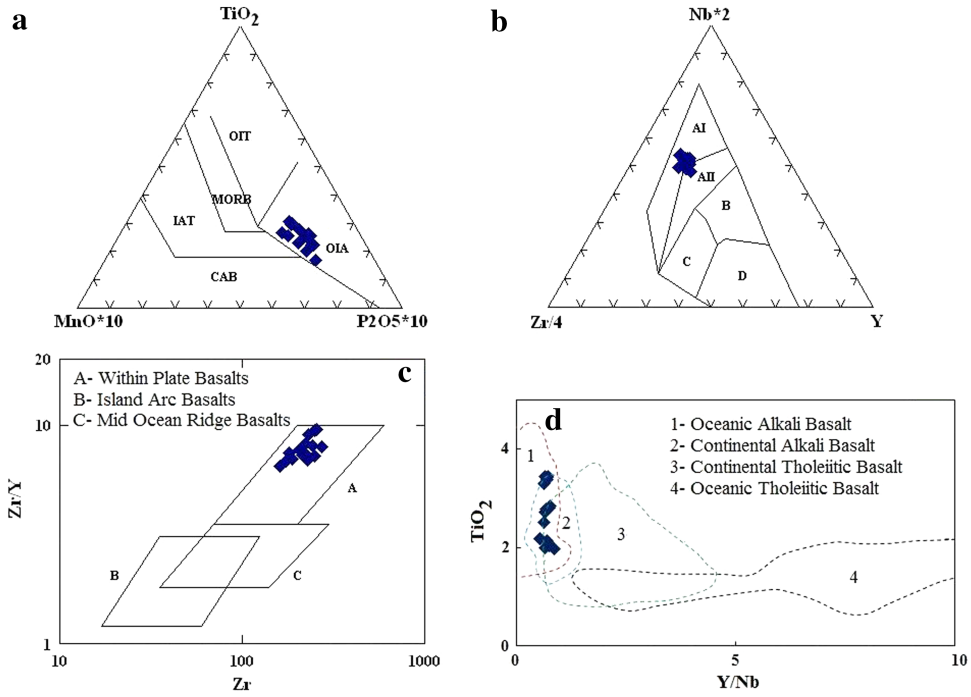

Fig. 8 Tectonomagmatic discrimination diagrams **a** TiO_2-MnO*10-P_2O_5*10 (after Mullen 1983), **b** Zr/4-Y-Nb*2 diagram of Meschede (1986), **c** Z versus Zr/Y diagram of Pearce and Norry (1979), **d** TiO_2 versus Y/Nb (after Floyd and Winchester 1975). Explanation: *OIT* Oceanic Island Tholeiite, *OIA*, Oceanic Island Alkalic, *MORB* Mid-Ocean Ridge Basalt, *IAT*, Island Arc Tholeiite, *CAB* Island Arc Calc-Alkaline Basalts, *AI-AII* Within Plate Alkaline Basalts, *AII-C* Within Plate Tholeiites, *B* Mid-Ocean Ridge Basalts, *D* Mid-Ocean Ridge Basalts, *C-D* Volcanic Arc Basalts

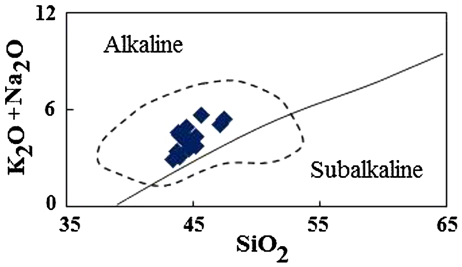

Fig. 9 Binary diagram of $Na_2O + K_2O$ versus SiO_2 (After Irvine and Baragar 1971). Explanation of the symbols given in Fig. 1. The *dashed* area of the Miocene-to-recent alkaline (East-of-Aden) Yemen Volcanic Series hosts the alkali basalt (*blue diamond*) of the Harrat Al-Birk

6 Discussion

6.1 Magmatic affinity and tectonic environment

Figure 10d introduces the Zr/Y ratio relative to Zr, as a fractionation index. In this diagram, the Harrat Al-Birk basalts plot in the intra-plate field, with remarkably higher Zr/Y ratios than MORB and island arc basalts (El-Akhal 2004). This characterization supports the alkaline nature of all samples and the comparability with most intra-plate basalts (Pearce and Cann 1973; Floyd and Winchester 1975). Figure 9 displays the patterns of the studied basalt and of the East of Aden alkaline Yemen Volcanic Series (YVS), which consists of mafic litho-types only with alkaline connotation, and does not show a transitional character like the West of Aden–East of Aden alkaline YVS. Both types of the alkaline YVS are characterized by a within-plate continental setting which is identical to the studied basalts. Thus, a within-plate setting seems to be more reasonable regardless of the source of magma, as will be shown in the next section.

6.2 Fractionation, magma type and its source

The negative correlations between SiO_2 and CaO, TiO_2 (Fig. 4) may suggest that the fractionation of clinopyroxene and ilmenite played a significant role in the process of formation (El-Hasan and Al-Malabeh 2008; Mao et al. 2014). Figure 5 shows positive correlation only of CaO against MgO, while the rest (Al_2O_3, Na_2O, K_2O, P_2O_5, and TiO_2 against MgO) are negatively correlated. This follows the other Saudi Arabian alkaline basalts in tracing the post-rift Miocene-to-recent YVS distribution pattern (Fig. 9; Mattash et al. 2013). This consequently indicates olivine and plagioclase fractionation that yields a consistent decline in CaO and Al_2O_3 with the decrease of MgO, and also the CaO decline indicates clinopyroxene fractionation in the most evolved basalts. The distribution of trace elements (Table 1) in the primary magma might be generated by partial melting of upper-mantle material, with possible involvement of crystallization processes that yield olivine and pyroxene (BanyYaseen et al. 2010).

Highly crustal-contaminated basalts are indicated by strong enrichment of alkali elements and result in high alkali/Nb ratios (Meshesha and Shinjo 2007), but this is not observed in the alkali basalt from the Harrat Al-Birk.

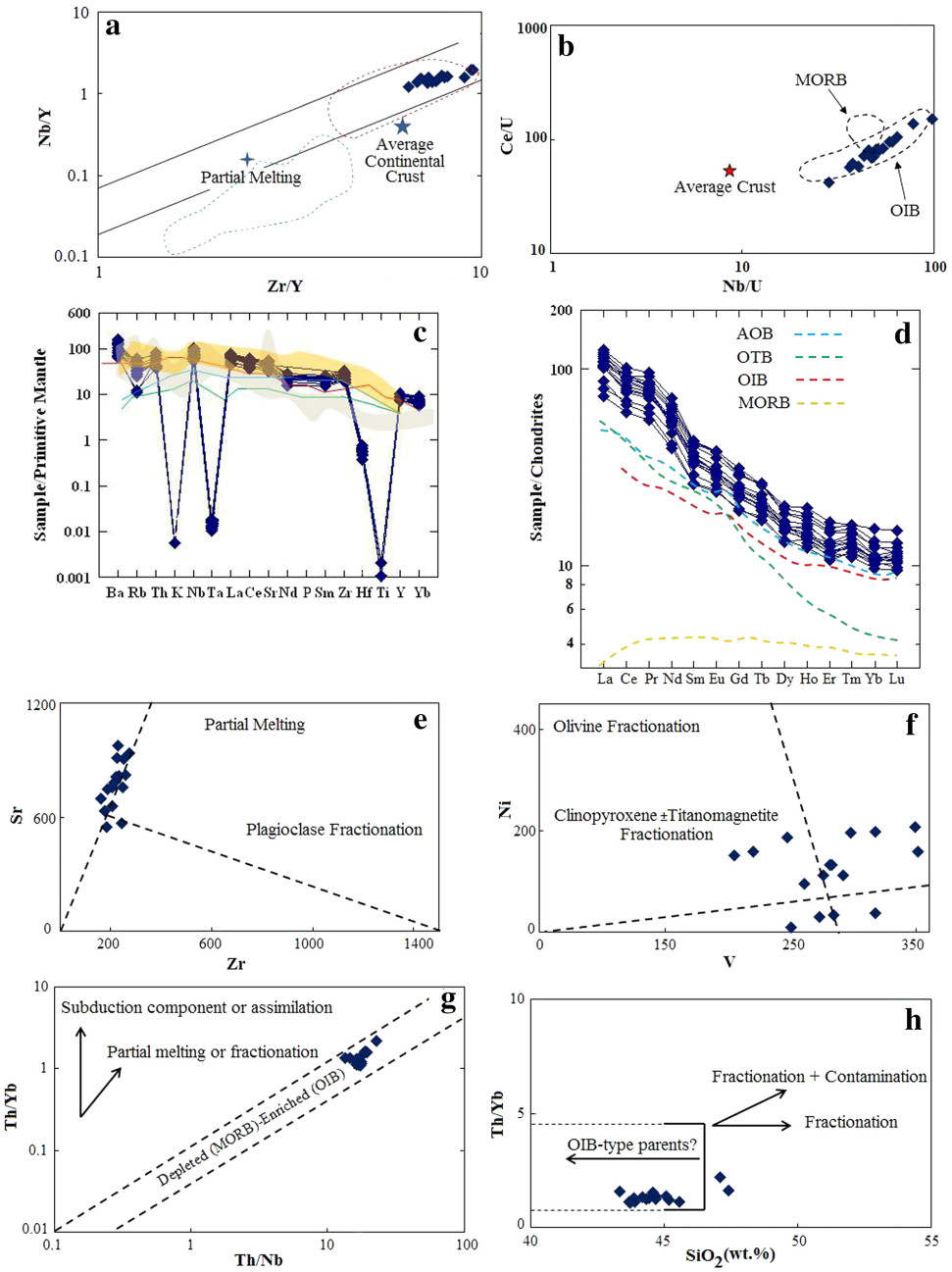

Fig. 10 Petrogenesis diagrams of the Harrat Al-Birk volcanic **a** Nb/Y versus Zr/Y variation diagram showing that the studied basalts plot in the ocean island basalt (OIB) field (*dashed-red line*); OIB field from Fitton and James (1986) and N-MORB from Fitton et al. (1997, 2003). The *+symbol* represents an estimate of primitive mantle composition (McDonough and Sun 1995). Average crust composition is from Rudnick and Fountain (1995) and Barth et al. (2000). **b** Ce/U versus Nb/U (after Moghazi 2003) compared with MORB average crust (Ito et al. 1987; Hofmann et al. 1986) and OIB (Hofmann et al. 1986; Davies et al. 1989). **c** Primitive mantle-normalized trace element diagram (normalization values from Sun and McDonough 1989). Source of the Iranian Cenozoic continental collision basalts of Nayband/Neh data (*light gray area*) and the OIB trend (*red line*) form Kheirkhah et al. (2015), and the African basalts data (*light orange area*), the alkali olivine basalts (*sky blue line*), and the olivine tholeitic basalts (*green line*) data from Camp and Roobol (1989). **d** Chondrite-normalized REE patterns. Nakamura (1974), average OIB (Sun and McDonough 1989), average N-type MORB (Sun and McDonough 1989), OTB and the AOB analyses from Camp and Roobol (1989). **e** Sr versus Zr and **f** Ni versus V for Possible partial melting and fractionation paths (from Camp and Roobol 1989). **g** Th/Yb versus SiO_2 and **h** Th/Yb versus Nb/Yb (after Pearce and Peate 1995)

Therefore, it is suggested that there is no crustal contamination effect on the original evolved magma. The studied alkaline basalt shows Ti enrichment which could be attributed to low melting degrees of the peridotite source rock (Shehata and Theodoros 2011). K_2O-poor magma from a water-saturated melting (e.g. Beard and Lofgren

1989; Thy et al. 1990; Beard and Lofgren 1991) is consistent with the Harrat Al-Birk volcanics, and therefore a water-saturated melt origin cannot be discarded in the petrogenesis of rift-related volcanics in the western Arabian Peninsula. From the comparison shown in Fig. 10d, the Harrat Al-Birk basalts have REE patterns similar to those of AOB (Camp and Roobol 1989) and OIB (Sun and McDonough 1989).

The trace elements diagram for the primitive mantle–normalized basalts shows that the Harrat Al-Birk basalts have very distinct negative anomalies of K, Ta, and Ti, and very small positive ones for Nb and Zr; this is characteristic of the Tertiary-to-recent continental alkali basalts (Norry and Fitton 1983) that are derived from asthenospheric materials (Thompson 1986; Wilson 1989). For comparison, some reference data are used, namely the primitive mantle–normalized traces of the studied basalts and the average of Iranian Cenozoic continental collision basalts (Kheirkhah et al. 2015); the average of African basalts (Camp and Roobol 1989) and the pattern of the oceanic island basalts; and the alkali olivine basalts (Kheirkhah et al. 2015) and the olivine tholeiitic basalts (Camp and Roobol 1989). The comparison reveals that the trend of the studied basalts follows well that of the OIBs and is very similar to that of the AOBs, but differs from the transitional tholeiite basalts. According to Meshesha and Shinjo (2007), the latter is characterized by flat patterns with small negative anomalies of Th and Nb-T, and positive anomalies of Ba and Pb. Strong depletion in Ti may indicate fractional crystallization of ilmenite, and the depletion in Ti and K indicates fractionation that most likely involves ilmenite-magnetite and feldspar minerals with almost no crustal addition due to the absence of any negative anomalies of Nb and Ta (Ahmad and Chaudhry 2008). The K depletion may also suggest the occurrence of residual amphibole ± phlogopite in the mantle source of basalts (Ulrych et al. 2010). The ratios of Ce/U and Rb/Sr are very useful as they can assist in distinguishing mantle sources from crustal ones (Hofmann et al. 1986; McDonough 1990). The Harrat Al-Birk basalts show a relatively lower Ce/U as compared to MORB, and samples mostly plot in the OIB field in Fig. 10b, h, in addition to fitting well with Fig. 10a, c. This strongly suggests an oceanic island mantle source for the studied basalts. In Fig. 10d, the REE pattern of these basalts seems to be very similar to that of OIBs and AOBs. Also, in Fig. 10d, it appears that the fractionation process is not extensive. The effect of such a process appears in Fig. 10f, where some samples follow the clinopyroxen ± titanomagnetite fractionation trend and do not show clear compatibility with the olivine trend. The petrogenesis diagrams also indicate that the source of the studied basalts was not modified by any contamination or assimilation (Fig. 10g, h). The source of the Harrat Al-Birk basalts is then an enriched oceanic island basaltic melt (Fig. 10g) that resulted from either subducted continental mantle lithosphere or a mantle metasomatism of subducted oceanic lithosphere (Niu et al. 2012).

7 Conclusions

Geochemical analysis indicated that the studied rocks of the Harrat Al-Birk are low- to medium-Ti, sodic-AOB with an enriched oceanic island signature but extruded in a within-plate environment. The rocks mainly formed by partial melting with a slight effect of crystal fractionation, which was most likely dominated by clinopyroxene and iron oxides (titanomagnetite, ilmenite).

The studied basalts are characterized by enrichment of light REEs and depletion in Ba, Th and K, Ta, and Ti. It is suggested that the magma source that generated the volcanic rocks of Harrat Al-Birk was a silica under-saturated water-saturated melt origin, dominantly evolved by partial melting of asthenospheric upper mantle in the form of an enriched oceanic island source (either subducted continental mantle lithosphere or a mantle metasomatism of subducted oceanic lithosphere, possibly peridotite with some hydrous silicates), involving some fractional crystallization yielding olivine, pyroxene (significant affect of clinopyroxene fractionation in basalts), amphiboles, ilmenite, and plagioclase.

Acknowledgments This work was funded by the Deanship of Scientific Research (DSR), King Abdulaziz University, Jeddah, under Grant No. (D1435-710-145) The authors, therefore, gratefully acknowledge DSR technical and financial support. The author is greatly indebted to the fruitful discussions by Prof. Adel Surour and Dr. Kamal Ali that improved the quality of work.

References

Ahmad SA, Chaudhry MN (2008) KiranaVolcanics, Pakistan-geochemical characterization and origin. Geol Bull Punjab Univ 43:49–57

Baker PE, Brosset R, Gass I (1973) Jebel al Abyad: a recent in western Saudi Arabia. Lithos 6:291–314

BanyYaseen IA, Al-Hawari Z, Diabat AA (2010) Petrology, geochemistry, petrogenesis and reactivation of volcanic tuffs at Dair El-Kahif Area, NE-Jordan. J Civil Eng 4:336–350

Barth MG, McDonough WF, Rudnick RL (2000) Tracking the budget of Nb and Ta in the continental crust. J Chem Geol 165:197–213

Beard JS, Lofgren GE (1989) Effect of water on the composition of partial melting of greenstone and amphibolite. Science 244:195–197

Beard JS, Lofgren GE (1991) Dehydration melting and water-saturated melting of basaltic and andesitic greenstone and amphibolites at 1, 3, and 6.9 kb. J Petrol 32:365–401

Brown GF, Schmidt DL, Huffman AC (1989) Geology of the Arabian peninsula: Shield area of western Saudi Arabia. United States Geological Survey, Professional paper 560-A, p 188

Camp VE, Roobol MJ (1989) The Arabian continental alkali basalt province: part I. Evolution of HarratRahat, Kingdom of Saudi Arabia. Geol Soc Am Bull 101:71–95

Coleman, RG, Fleck RJ, Hedge CE, Ghent ED (1977) The volcanic rocks of southwest Saudi Arabia and the opening of the Red Sea, In Hilpert, LS (ed) Red sea Research, 1970–1975: Saudi Arabian Directorate of Mineral Resources, Bull no. 22, pp 1–20

Coleman RG, Gregory RT, Brown GF (1983) Cenozoic volcanic rocks of Saudi Arabia, United States Department of the Interior Geological Survey, Open-File Report 83–788, p 82

Davies GR, Norry MJ, Geralch DC, Cliff R A (1989) A combined chemical and Pb–Sr–Nd isotope study of the Azores and cape verde hot-spots: the geodynamic implications. In: Saunders AD, Norry MJ (eds) Magmatism in the ocean basins. Geological Society of London, Special Publication No 22, pp 231–256

El-Akhal H (2004) Contribution to the petrography, geochemistry, and tectonic setting of the basalt flows of the Umm-Qais plateau, north Jordan. Geol Bull Turk 47:1–10

El-Hasan T, Al-Malabeh A (2008) Geochemistry, Mineralogy and Petrogenesis of El-Lajjoun Pleistocene Alkali Basalt of Central Jordan. Jordan J Earth Environmental Sci 1(2):53–62

Fitton JG, James D (1986) Basic volcanism associated with intraplate linear features. Philos Trans R Soc Lond A317:253–266

Fitton JG, Saunders AD, Norry MJ, Hardarson BS, Taylor RN (1997) Thermal and chemical structure of the Iceland plume. Earth Planet Sci Lett 153:197–208

Fitton JG, Saunders AD, Kempton PD, Hardarson BS (2003) Does depleted mantle form an intrinsic part of the Iceland plume? Geochem Geophys Geosyst 4:Q01032. doi:10.1029/2002GC000424

Floyd PA, Winchester JA (1975) Magma type and tectonic setting discrimination using immobile elements. Earth planet Sci Lett 27:211–218

Ghent ED, Coleman RG, Hadley DG (1979) Ultramafic Inclusions and Host Alkali Olivine Basalts of the Southern Coastal Plain of the Red Sea, Kingdom of Saudi Arabia. U. S. Geological Survey, Saudi Arabian Project Report 244, p 1339

Healy JH, Mooney WD, Blank HR, Gettings ME, Kohler WM, Lamson RJ, Leone LE (1982) Saudi Arabian seismic deep-refraction profile: final project report: Saudi Arabian Deputy Ministry for Mineral Resources Open-File Report USGS-OF-02-37, p 429

Hofmann AW, Jochum KP, Seufert M, White WM (1986) Nb and Pb in oceanic basalts: new constraints on mantle evolution. Earth Planet Sci Lett 79:33–45

Irvine TN, Baragar WRA (1971) A guide to the chemical classification of the common volcanic rocks. Can J Earth Sci 8:523–548

Ito E, White WM, Göpel C (1987) The O, Sr, Nd and Pb isotope geochemistry of MORB. Chem Geol 62(3–4):157–176

Kheirkhah M, Neill I, Allen MB (2015) Petrogenesis of OIB-like basaltic volcanic rocks in a continental collisionzone: Late Cenozoic magmatism of Eastern Iran. J Asian Earth Sci 106:19–33

Le Bas MJ, Le Maitre RW, Streckeisen A, Zanettin B (1986) A chemical classification of volcanic rocks based on the total alkali-silica diagram. J Petrol 27:745–750

Mao Q, Xiao W, Fang T, Windley BF, Sun M, Ao S, Zhang J, Huang X (2014) Geochronology, geochemistry and petrogenesis of Early Permian alkaline magmatism in the Eastern Tianshan: implications for tectonics of the Southern Altaids. Lithos 190–191:37–51

Mattash MA, Pinarelli L, Vaselli O, Minissale A, Al-Kadasi M, Shawki MN, Tassi F (2013) Continental flood basalts and rifting: geochemistry of Cenozoic Yemen Volcanic Province. Int J Geosci 4:1459–1466

McDonough WF (1990) Constraints on the composition of the continental lithospheric mantle. Earth Planet Sci Lett 101(1):1–18

McDonough WF, Sun S (1995) The composition of the Earth. J Chem Geol 120:223–253

McGuire AV (1988) The mantle beneath the Red Sea margin: xenoliths from western Saudi Arabia. In: Bonatti E (ed) Zabargad Island and the Red Sea Rift. Tectonophysics, 150 (1–2): pp 101–119

Meschede M (1986) A method of discriminating between different types of mid-ocean ridge basalts and continental tholeiites with the Nb-Zr-Y diagram. J Chem Geol 56:207–218

Meshesha D, Shinjo R (2007) Crustal contamination and diversity of magma sources in the northwestern Ethiopian volcanic province. J Miner Petrol Sci 102:272–290

Middlemost E (1975) The basalt clan. Earth Sci Rev 11:337–564

Moghazi AM (2003) Geochemistry of a Tertiary continental basalt suite, Red Sea coastal plain, Egypt: petrogenesis and characteristics of the mantle source region. Geol Mag 140:11–21

Moufti MR, Hashad MH (2005) Volcanic hazards assessment of Saudi Arabian Harrats: geochemical and isotopic studies of selected areas of active Makkah–Madinah–Nafud (MMN) volcanic rocks. Final project Report (LGP-5-27), King Abdulaziz City for Science and Technology, Riyadh, p 401

Moufti MR, Matsah MI, Soliman MA, Moghazi AM (2011) Arabian plume dynamics beneath Al-Madinah Al-Munawwarah region and its related geohazards, Final project Report (ARP-26-79, King Abdulaziz City for Science and Technology, Riyadh, p 382

Moufti MR, Moghazi AM, Ali KA (2012) Geochemistry and Sr–Nd–Pb isotopic composition of the Harrat Al-Madinah volcanic field, Saudi Arabia. Gondwana Res 21:670–689

Moufti MR, Németh K, Murcia H, Lindsay JM, El-Masry N (2013) Geosite of a steep lava spatter cone of the 1256 AD, Al-Madinah eruption, Kingdom of Saudi Arabia. J Geosci 5(2):189–195

Mullen ED (1983) $MnO/TiO_2/P_2O_5$: a minor element discrimination for basaltic rocks of oceanic environments and its implications for petrogenesis. Earth Planet Sci Lett 62:53–62

Murcia H, Smith IEM, Lindsay JM, Moufti MR, Németh K, Cronin SJ, El-Masry NN (2013) Geochemistry of the most-recent, dominantly effusive volcanism in northern Harrat Rahat. Vorisa Sci Meet 17–18:39–43

Nakamura K (1974) Determination of REE, Ba, Fe, Mg, Na and K in carbonaceous and ordinary chondrites. Geochem Cosmochim Acta 38:757–775

Nasir S, Stern RJ (2012) Lithospheric petrology of the eastern Arabian Plate: constraints from Al-Ashkhara (Oman) xenoliths. Lithos 132–133:98–112

Nemeth K, El-Masry N, Moufti MR (2014) The Pleistocene Jabal Akwa Al Yamaniah maar/tuff ring-scoria cone complex as an analogy for future phreatomagmatic to magmatic explosive eruption scenarios in the Jizan Region, SW Saudi Arabia. Balkan Geological Association Congress at Tirana, Albania pp 243–246

Niu Y, Wilson M, Humphreys ER, O'Hara MJ (2012) A trace element perspective on the source of ocean island basalts (OIB) and fate of subducted ocean crust (SOC) and mantle lithosphere (SML). Episodes 35:310–327

Norry MJ, Fitton JG (1983) Compositional differences between oceanic and continental basic lavas and their significance. In: Hawkesworth CJ, Norry MJ (eds) Continental basalts and mantle xenoliths. Shiva Publishing Ltd., Cheshire, pp 5–19

Pearce JA, Cann JR (1973) Tectonic setting of basic volcanic rocks determined using trace element analysis. Earth planet Sci Lett 19:290–300

Pearce JA, Norry MJ (1979) Petrogenesis implications of Ti, Zr, Y, and Nb variations in volcanic rocks. Cont Miner Petrol 69:33–47

Pearce JA, Peate DW (1995) Tectonic implications of the composition of volcanicarc magmas. Annu Rev Earth Planet Sci Lett 23:251–285

Ross DA, Whitmarch RB, Ali SA, Boudreaux JE, Coleman RG, Fleisher RL, Girdler R, Manheim F, Matter A, Nigrini C, Stoffers P, Supko PR (1973) Red Sea drillings. Science 179:377–380

Rudnick RL, Fountain DM (1995) Nature and composition of the continental-crust—a lower crustal perspective. Rev Geophys 33:267–309

Shehata A, Theodoros N (2011) Alkali basalt from Burgenland, Austria: petrological constraints on the origin of the western most magmatism in the Carpathian-paunonian Region. Lithos 121:176–188

Sun SS, McDonough WF (1989) Chemical and isotopic systematic of oceanic basalts: implicattions for mantle composition and process. In: Sauders AD, Norry MJ (eds) Magmatism in the ocean basins. Geological Society Special Publication No. 42, pp 313–345

Surour AA, Moufti M (2013) Opaque mineralogy as a tracer of magmatic history of volcanic rocks: an example from the Neogene-Quaternary HarratRahat intercontinental volcanic field, north western Saudi Arabia. Acta Geol Sin (English Edition) 87:1281–1305

Thompson R (1986) Sources of basic magmas. Nature 319:448–449

Thy P, Beard JS, Lofgren GE (1990) Experimental constraints on the origin of icelandic rhyolites. J Geol 98(3):417–421

Ulrych J, Jelınek E, Randa Z, Lloyd FE, Balogh K, Hegner E, Novák J (2010) Geochemical characteristics of the high- and low-Ti basaltic rocks from the uplifted shoulder of the Ohře (Eger) Rift, Western Bohemia. Chem Erde 70:319–333

Wilson M (1989) Igneous petrogenesis, a global tectonic approach. Unwin Hyman 466 p

Winchester JA, Floyd PA (1977) Geochemical discrimination of different magma series and their differentiation products using immobile elements. J Chem Geol 20:325–343